Frontiers of Physics
https://doi.org/10.1007/s11467-018-0864-1
Front. Phys.
14(2), 23601 (2019)

RESEARCH ARTICLE

Dynamics of the phase-change material GeTe across the structural phase transition

T. Chatterji[1], S. Rols[1], U. D. Wdowik[2,†]

[1] *Institut Laue-Langevin, 71 avenue des Martyres, 38000 Grenoble, France*
[2] *Institut of Technology, Pedagogical University, Podchorazych 2, PL-30-084 Krakow, Poland*
Corresponding author. E-mail: [†] *sfwdowik@cyf-kr.edu.pl*
Received May 8, 2018; accepted September 10, 2018

Results of inelastic neutron scattering experiments and *ab initio* molecular dynamics simulations for GeTe – the parent compound of phase-change materials are reported. The inelastic neutron spectra of GeTe powder samples have been determined in the temperature range extending from 300 to 700 K. The phonon peaks undergo thermal shifts resulting from anharmonic effects being weaker for acoustic than optic modes. A small concentration of free charge carries arising from the presence of Ge-vacancies was found not to affect significantly the neutron weighted phonon densities of states of GeTe. The spectral pattern changes qualitatively across the structural phase transition, but the local structure of GeTe remains hardly affected, as confirmed by the analysis of temperature dependence of the pair-distribution function obtained from *ab initio* molecular dynamics investigations. The present theoretical studies support in a wide extent our experimental observations and also those provided by local probe methods.

Keywords phase-change materials, inelastic neutron scattering, *ab initio* molecular dynamics

1 Introduction

Unique properties of phase-change materials from the ternary Ge-Sb-Te system enabled effective utilization of $(GeTe)_m(Sb_2Te_3)_n$ (GST) compounds in a diverse data storage devices [1] as well as open a route for their application in modern non-volatile random access memories (non-volatile RAM) [2, 3]. These materials are known for the rapid and reversible transformation between their amorphous and crystalline states that vastly differ in their electrical and optical properties. The crystalline-to-amorphous phase transition in GST materials, i.e., switching of their physical properties is usually induced by laser pulses (laser heating) or current pulses (Joule heating) [2].

Despite successful application of the GST materials in optical data storage devices (CDs, DVDs and blue-ray disks) and some attempts to employ them in non-volatile RAM devices, a comprehensive understanding of mechanism underlying the phase transitions in these compounds is still lacking. A typical example is the temperature induced structural phase transition in GeTe. Although this parent compound of the GST phase-change materials has been hotly debated since the seminal work of Steigmeier *et al.* [4], the driving force of the rhombohedral-to-cubic phase transformation at $T_c \sim 600$ K along with accompanying effects still remain a source of controversy in spite of numerous experimental [5–14] and theoretical [15–22] studies carried out on crystalline and amorphous phases as well as stoichiometric and non-stoichiometric samples. In particular, an ambiguity refers to (i) disappearance or persistence (in the nanometer local scale) of the Peierls distorted Ge-Te bonds above T_c which are characteristic for the low-temperature ferroelectric rhombohedral phase of the $R3m$ symmetry, (ii) the nature of phase transition (displacive or order-disorder) and its kind (first or second order), and (iii) detailed explanation of the volume contraction at T_c.

Generally, the spectroscopic methods, including neutron diffraction [5, 11] and the Raman scattering [4, 9], clearly indicate for vanishing structural lattice distortions and formation of the paraelectric rock-salt phase with a single Ge-Te bond above transition temperature. Results of these experiments are supported by the recent *ab initio* phonon calculations [20] which provide microscopic mechanism underlying the structural phase transition in crystalline GeTe and confirm its displacive nature. Quite different picture emerges, however, from the so-called local probes, such as the extended X-ray-absorption fine structure (EXAFS) experiments [6] and the pair distribution function (PDF) analysis of the X-ray diffraction data [7, 10]. They both observe two distinct Ge-Te bonds in the high-temperature paraelectric phase of $Fm\bar{3}m$ symmetry which hardly change across the phase transition. Based on these findings the displacive nature of the structural $R3m \leftrightharpoons Fm\bar{3}m$ phase transformation in GeTe has been

questioned and suggested to be of the order-disorder type.

This work addresses inelastic neutron scattering (INS) experiments on powder GeTe samples and *ab initio* molecular dynamics (AIMD) simulations which have been undertaken to revisit lattice dynamics of GeTe as a function of temperature and examine behavior of the local versus average structure of this compound across the structural phase transition.

2 Experimental and calculation details

The GeTe powder samples of 99.999% purity and 200 mesh (74 μm) were purchased from Alfa Aesar. They were additionally verified for contaminating phases by the X-ray powder diffraction (for details see Ref. [11]). These measurements revealed a very small amount of GeO_2 impurity phase. The sample of about 5 g was used in the INS experiments performed on the time-of-flight spectrometer IN4C mounted on the thermal neutron beam of the Institut Laue–Langevin in Grenoble, France. The INS spectra were measured at several temperatures between 300 and 700 K with incident neutron energy $E_i = 14.34$ meV. The data were corrected for scattering of the sample holder and normalized to vanadium. Resulted signal was transformed into the so-called generalized density of states $G_D(E)$, i.e., the quantity which is usually extracted from the measured scattering function [23]. In the framework of incoherent approximation [24] and after proper averaging of the scattered signal over a wide range of scattering angles (120°) provided by the IN4C multidetector, the $G_D(E)$ can be expressed as [25, 26] $G_D(E) = \sum_{\mu}^{N} c_\mu \frac{\sigma_\mu}{M_\mu} g_\mu(E)$, where the sum runs over all atoms in the unit cell. The symbols c_μ, σ_μ, M_μ and $g_\mu(E)$ denote respectively concentration, total coherent scattering cross section [27], mass, and partial phonon density of states for the μth atomic species. Details of the data analysis can also be found elsewhere [28].

Ab initio molecular dynamics (AIMD) calculations were performed within density functional theory (DFT) method implemented in the Vienna *ab Initio* Simulation Package (VASP) [29–31]. Generalized gradient approximation (GGA) in the PBE parametrization [32, 33] for the exchange-correlation functional and the projector augmented wave (PAW) [34, 35] pseudopotentials were applied. The $Ge(4s^24p^2)$ and $Te(5s^25p^4)$ electrons were treated as valence electrons. A plane wave basis set with an energy cutoff of 228 eV and a grid of $2 \times 2 \times 2$ k-points for integration over the Brillouin zone were used in all calculations. Simulations were carried out at 300, 400, 500, 600 and 700 K using canonical (NVT) ensemble with a Nosé thermostat. The low- and high-temperature phases were modeled by supercells containing respectively 128 and 216 atoms. The volumes and initial configurations of the respective supercells were determined in our previous DFT studies [20]. For each temperature the system was first equilibrated for 18 ps and subsequently simulated for 30 ps with a time step of 3 fs. To check the effect of supercell size on the simulated generalized densities of phonon states, additional calculations were performed at 500 K in the supercell of volume corresponding to the crystal volume determined at 500 K in our previous high-resolution neutron powder diffraction (NPD) experiments [11]. Due to a numerous experimental/theoretical observations indicating the presence of native points defects (Ge-vacancies) in GeTe, we have simulated the $G_D(E)$ spectrum of non-stoichiometric $Ge_{1-x}Te$ with $x = 1.6\%$ at 500 K. The assumed x approximates the experimental value of the free charge carriers concentration [17, 18] of about 10^{21} holes/cm^3. The $Ge_{1-x}Te$ structure with $x = 1.6\%$ was modeled by taking out one Ge atom from the initial 128-atomic supercell.

Phonon densities of states were obtained from a Fourier transform of the atomic velocity autocorrelation function [36] $D(\omega) = \int_0^T \frac{\langle \sum_{j=1}^{N} \boldsymbol{v}_j(t)\boldsymbol{v}_j(0)\rangle}{\langle \sum_{j=1}^{N} \boldsymbol{v}_j(0)\boldsymbol{v}_j(0)\rangle} \exp(-\mathrm{i}\omega t)\mathrm{d}t$, where $\boldsymbol{v}_j(t)$ is the velocity vector of atom j at the time t obtained from AIMD simulations. To better compare with results of the INS experiments, the calculated densities of phonon states have been neutron-weighted [25–27] and convoluted with the instrumental resolution. Pair distribution functions $G(r)$ were simulated using the nMOLDYN software [37]. The wave-vector projected power spectra of the autocorrelation function $G_{\boldsymbol{q}}(\omega)$ were calculated following the formalism given in Refs. [38, 39].

3 Results and discussion

In general, the $G_D(E)$ spectra for GeTe are inherently weighted heavily toward Ge atom scattering due to its more than three times higher scattering efficiency (0.118 barn/a.m.u.) than that of Te atom (0.034 barn/a.m.u.). Thus, the neutron weighted phonon densities of states at each temperature remain more sensitive to vibrations of the Ge-sublattice which contributes about 78% to the total $G_D(E)$ spectrum. Temperature evolution of the experimental and theoretical neutron-weighted densities of phonon states in GeTe which is presented in Fig. 1 clearly indicates that below $T_c \sim 600$ K the spectra consist of three phonon bands covering the energy range up to 24 meV. The lowest frequency band extending to 11 meV is composed of two peaks corresponding to acoustic phonons which involve the transverse (TA) and longitudinal (LA) modes. The transverse optic (TO) modes constitute the medium frequency band ranging from 12 to 18 meV, while the longitudinal optic (LO) modes give rise to the highest frequency band. A small peak at 27 meV appearing in the room temperature spectrum melts away upon heating, and thus we do not assign it to any phonon mode characteristic for the low-temperature GeTe phase, since it has not been detected in our previous INS experiments

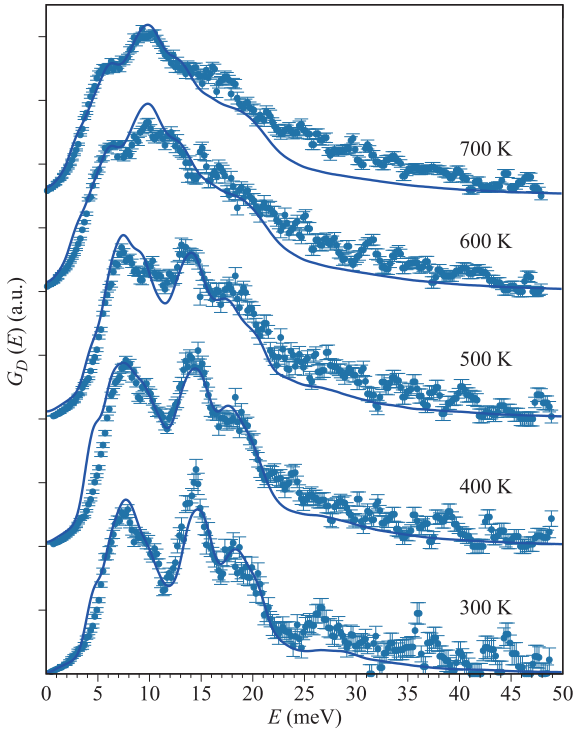

Fig. 1 Neutron weighted phonon density of states $G_D(E)$ of GeTe from INS experiments (circles) and AIMD simulations (curves) at selected temperatures. The INS spectra were measured at incident energy $E_i = 14.34$ meV (2.4 Å). Experimental and calculated $G_D(E)$ are normalized to unity.

[20] performed at 150 K. Therefore, its origin remains unknown at present.

Between 300 K and 600 K the spectra maintain their four-peak pattern which is very similar to that previously measured at 150 K and calculated at the ground state [20]. Both acoustic and optic bands undergo thermal shifts downward the energy scale upon heating. The temperature shift of peaks belonging to the acoustic band is, however, smaller than that for peaks constituting the optic band. A shifting of the spectral peaks to lower frequencies is assisted by the peaks broadening. Again, the increase of line widths is much more noticeable for the high-frequency peaks from the optic band. In the vicinity of rhombohedral-to-cubic phase transition the four-peak $G_D(E)$ structure evolves toward a three-peak one and the latter pattern can be recognized until the highest temperature of 700 K.

The thermal shifts of phonon frequencies can be assigned to intrinsic and extrinsic lattice anharmonicity [38, 39]. The latter contribution is usually due to thermal expansion of the system lattice. In order to resolve which of these effects dominates in GeTe, we have recalculated the $G_D(E)$ spectrum at 500 K using the experimental volume (V_{EXP}) of GeTe determined at this temperature in our recent high-resolution NPD experiments [11]. Resulting $G_D(E)$ spectrum is compared to that simulated for the ground state volume (V_0) in Fig. 2. Apart from the lower (higher) intensity of the acoustic (transverse optic) peaks and small downward shift of the acoustic modes at V_{EXP}, no significant difference between the spectral patters obtained at V_0 and V_{EXP} is observed. Such a small shift of the acoustic phonons is associated with the 2% increase of V_{EXP} with respect to V_0. We should also note the volume dilation of less than 1% between 300 and 500 K, as evidenced from our recent high-resolution NPD measurements and the quasi-harmonic calculations [11].

More pronounced modifications of the generalized phonon densities of states, which are visible especially in the middle frequency band constituted by the optical modes, are found for the $Ge_{1-x}Te$ with $x = 1.6\%$. Figure 2 shows that incorporation of vacancies into the Ge-sublattice yields a slight splitting of TO band into two peaks, while leaving the acoustic band practically unchanged. We note that similar observation indicating a very weak influence of free charge carriers on the acoustic phonons of GeTe follows from the previous lattice dynamical calculations [17] performed at the ground state. The latter predict, however, some softening of the optical phonon frequencies in the GeTe system doped with $\sim 2.1 \times 10^{21}$ holes/cm^3, which is rather not observed in our AIMD studies. The downshift of optical phonon band reported by Shaltaf *et al.* [17] might be an artifact associated with the applied methodology, in which Ge-vacancies were not explicitly treated, but their effect was mimic by a change of the number of electrons counterbalanced by a background. In contrast, our AIMD calculations take into account the effect of real Ge-vacancies which are created in the Ge-sublattice by removing the appropriate number of Ge atoms from the simulated supercell to maintain required concentration of these defects ($x = 1.6\%$). Due to a rather minor effect of both Ge-vacancies and the ther-

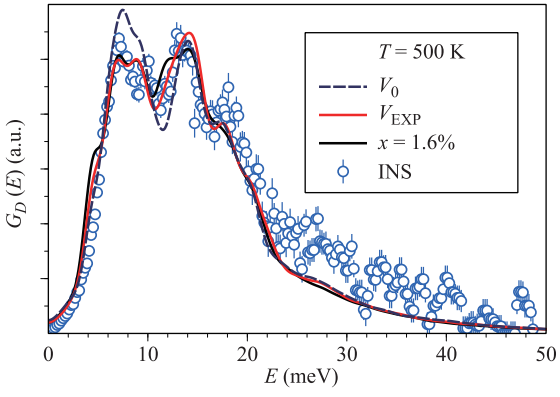

Fig. 2 The INS (open symbols) and AIMD (curves) neutron weighted phonon densities of states of GeTe and $Ge_{1-x}Te$ ($x = 1.6\%$) at 500 K. Simulations for the ideal and defected GeTe lattice are performed at the experimental volume (V_{EXP}) determined in our previous NPD measurements [11]. The INS spectra are measured at $E_i = 14.34$ meV (2.4 Å). The $G_D(E)$ spectra are normalized to unity.

mal expansivity on the neutron weighted phonon densities of states of GeTe, we limit our further discussion to the results obtained for the defect-free lattice at the volume V_0.

To gain a deeper insight into the observed changes, we have projected the AIMD power spectra of the autocorrelation function onto the selected wave-vectors which are commensurate with the supercell size. Although such spectra contain contributions from all vibrational modes with the wave vector $\boldsymbol{q}$, they allow us to better resolve individual phonons. The resulting projected spectra at the $\Gamma(0,0,0)$, $F(0,\frac{1}{2},\frac{1}{2})$, $T(\frac{1}{2},\frac{1}{2},\frac{1}{2})$ and $L(\frac{1}{2},0,0)$ high-symmetry points of the $R3m$ structure of GeTe determined between 300 K and 500 K are shown in Fig. 3(b).

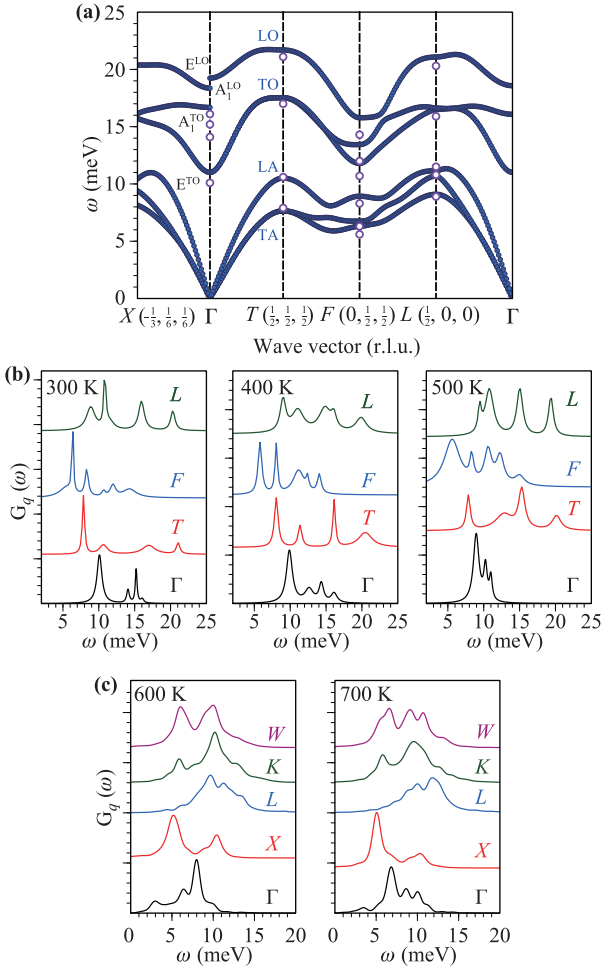

Fig. 3 **(a)** Phonon dispersion relations of the rhombohedral GeTe at the ground state [20]. Open symbols denote calculated frequencies at 300 K. **(b)** Wave vector projected power spectra of the autocorrelation function $G_{\boldsymbol{q}}(\omega)$ onto the $\Gamma(0,0,0)$, $T(\frac{1}{2},\frac{1}{2},\frac{1}{2})$, $F(0,\frac{1}{2},\frac{1}{2})$, and $L(\frac{1}{2},0,0)$ high-symmetry points of the low-temperature $R3m$ structure of GeTe at 300, 400, and 500 K. **(c)** Wave vector projected power spectra of the autocorrelation function $G_{\boldsymbol{q}}(\omega)$ onto the $\Gamma(0,0,0)$, $X(\frac{1}{2},\frac{1}{2},0)$, $L(\frac{1}{2},\frac{1}{2},\frac{1}{2})$, $K(\frac{3}{8},\frac{3}{8},\frac{3}{4})$, and $W(\frac{1}{4},\frac{1}{2},\frac{3}{4})$ high-symmetry points of the high-temperature $Fm\bar{3}m$ structure of GeTe at 600 K and 700 K.

The phonon band structure of rhombohedral GeTe with the $R3m$ symmetry consist of six branches constituted by three acoustic and three optic phonons, as indicated by the calculated [20] dispersion relations at $T = 0$ K which are presented in Fig. 3(a). There are two transverse and one longitudinal branch within each acoustic/optic region. In principle, the number of peaks appearing in the $G_{\boldsymbol{q}}(\omega)$ spectrum should correspond to a number of modes at a given wave vector $\boldsymbol{q}$. At the Γ-point, the rhombohedral GeTe phase shows non-degenerate A_1 and doubly degenerate E modes which are both Raman- and infrared-active due to the lack of inversion symmetry. The $A_1$and E phonons are related to vibrations of the Ge and Te sublattices along and perpendicular to the crystal threefold axis, respectively. In addition, the long-range macroscopic electrostatic field accompanying atomic displacements splits the infrared-active modes into transverse (E^{TO}, A_1^{TO}) and longitudinal (E^{LO}, A_1^{LO}) components. Hence, the $G_{\boldsymbol{q}}(\omega)$ spectrum at the Brillouin zone center consists of four peaks correlating with the respective TO and LO modes. In the direction parallel to the threefold crystal axis, i.e., along the Γ–T direction, both TA and TO modes remain doubly degenerate, and thus the $G_{\boldsymbol{q}}(\omega)$ spectrum at the T-point exhibits four peaks due to TA, LA, E^{TO} and A_1^{LO} phonons. Although six modes could be observed for the calculated band structure at the F-point, the projected spectrum consists, however, of five peaks because the TA phonons having frequencies close to each other are hardly resolved. Both TA modes produce the high-intensity peak at about 6 meV. The modes with only slightly different frequencies can also give rise to peak broadening or double-peak structure, like those found at ∼ 11 meV and ∼ 16 meV in the L-projected spectra. Here, the broad and almost unsplit peaks result from weakly separated TA/LA and TO modes.

Below the rhombohedral-to-cubic phase transition the peaks positions of the $G_{\boldsymbol{q}}(\omega)$ spectra experience shifts with increasing temperature. The temperature evolution of the Γ-projected spectrum, indicates a monotonic decrease in frequencies of the E^{TO}, E^{LO} and A_1^{TO} modes up to transition temperature and an abrupt drop of the A_1^{LO} mode frequency just above 400 K. These lead to a three-peak pattern of the Γ-projected spectrum at 500 K. We should note that softening of the E^{TO} and A_1^{LO} modes with temperature has been previously determined by the Raman spectroscopy experiments [4, 9] which revealed different rates of softening for the E and A_1 phonons. The latter mode was observed to soften more rapidly than the former one. Simultaneous softening of both modes was followed by their convergence into the triply degenerate mode of T_{1u} symmetry just above 500–550 K. A disappearance of the Raman-active phonons was a direct signature of the $R3m \leftrightharpoons Fm\bar{3}m$ transition as the T_{1u} mode of the high-temperature rocksalt phase of GeTe remains Raman-inactive. On one hand the thermal shift of the calculated E^{TO} phonon correlates well with that determined for the

E mode in the Raman experiments, but on the other hand there is insufficient correspondence between experimental and theoretical observations for the A_1^{LO} phonon mode. Discrepancies between the present simulations and experiments reach about 1 meV for the E^{TO} mode and almost 3–4 meV for the A_1^{LO} mode (see Table 1).

In the vicinity of $R3m \leftrightharpoons Fm\bar{3}m$ transition the wave vector projected $G_{\boldsymbol{q}}(\omega)$ spectra notably change their spectral pattern. The projections displayed in Fig. 3(c) show broad distributions which reflect behavior observed in the INS spectra at $T \geq 600$ K. Both experimental and theoretical results suggest that the optical phonon modes in GeTe appear to be much more anharmonic than the acoustic ones and this effect is associated with the intrinsic lattice anharmonicity.

Results of our AIMD simulations can also be confronted with those from local structure measurements [6, 7, 10], which report an existence of short and long Ge-Te bonds in the high-temperature cubic phase of GeTe and even in its liquid state [16]. To probe the temperature evolution of the local structure of GeTe, we have computed the pair distribution functions $G(r)$ and extracted the Ge-Te bond lengths. Figure 4 illustrates the temperature dependence of the calculated PDFs along with the behavior of short and long Ge-Te bonds with increasing temperature. For comparison, the lengths of short and long Ge-Te bonds determined from our recent high-resolution NPD measurements [11] are included as well. The NPD data show a gradual change of the short and long Ge-Te bonds below $T_c \sim 600$ K and their convergence into a unique bond length of about 3 Å at the onset of structural transformation. We should note that such a behavior of Ge-Te bond lengths as that provided by our NPD investigations remains in accordance with the results of earlier reports based on the standard neutron diffraction or Raman scattering experiments [4, 5, 9]. Below T_c, results of the NPD and AIMD studies are also consistent as the two-peak

Table 1 Frequencies of the E^{TO} and A_1^{LO} phonon modes in GeTe. Theoretical frequencies result from projections of the power spectra of autocorrelation function onto the Γ-point. Experimental data are taken from the Raman scattering experiments on single crystals [4] and nanocrystals of 500 nm thickness [9].

Mode	300 K	400 K	500 K
		AIMD	
E^{TO} (meV)	10.1	9.9	9.0
A_1^{LO} (meV)	16.4	16.1	10.9
		Steigmeier *et al.* [4]	
E^{TO} (meV)	11.2	10.5	9.7
A_1^{LO} (meV)	15.5	14.1	13.2
		Polking *et al.* [9]	
E^{TO} (meV)	10.3	9.7	9.3
A_1^{LO} (meV)	13.4	14.4	14.3

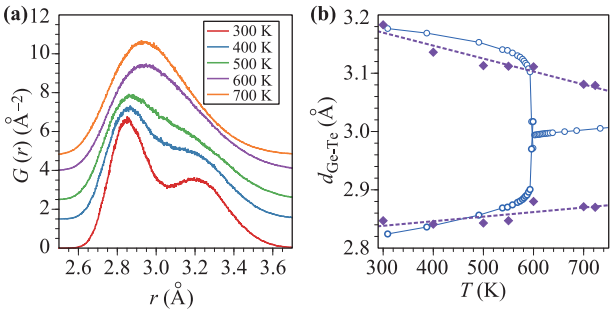

Fig. 4 **(a)** Pair-distribution function $G(r)$ of GeTe obtained from AIMD simulations at temperatures from 300 to 700 K in the range 2.5 to 4.0 Å corresponding to short and long Ge-Te bonds. **(b)** Temperature evolution of the Ge-Te bond lengths $d_{\text{Ge-Te}}$ extracted from the Gaussian fits to the calculated pair-distribution functions $G(r)$ (solid symbols) and determined from the neutron powder diffraction [11] (open symbols).

structure revealed by the calculated PDFs conforms to two distinct bond distances expected for the distorted rhombohedral phase of GeTe. This structure becomes washed out while approaching the phase transition and the resulting patterns at $T \geq T_c$ are characterized by an asymmetric broad peaks, in which one can still distinguish two Gaussians corresponding to two different bond lengths. This indicates an existence of structural distortions even above transition temperature, and hence confirms observations made with the EXAFS and PDF experiments [6, 7, 10, 16]. The structural distortions tend to diminish with increasing temperature, as evidenced by a slow convergence of the short and long bonds to a value representing single symmetry equivalent Ge-Te distance of the high-temperature cubic rocksalt phase or an average structure detected by conventional diffraction techniques [5, 11]. Such convergence is achieved at about 1400 K, i.e., well above the GeTe melting point of about 998 K. We should mention that similar value of transition temperature ($\sim$ 1700 K) has been estimated in the recent experimental investigations based on the PDF analysis of the high-energy X-ray total scattering data [10]. The average Ge-Te distance was found not to change significantly with temperature, but the atomic coordination became more symmetric above T_c. Thus, the present theoretical results reflect the behavior of the local GeTe structure observed using the methods commonly referred to as local probes.

4 Summary and conclusions

Generalized phonon densities of states of GeTe have been measured by INS and simulated by AIMD in temperatures ranging from 300 to 700 K. Results of AIMD simulations remain in accord with experimental observations. The softening of phonons upon temperature is more pronounced for modes belonging to the optical band than those from acoustic region, which signifies weaker an-

harmonicity of acoustic phonons as compared to optical modes. The optical modes may be to some extent sensitive to point defects such as Ge-vacancies and experience some shifts and splittings, but the acoustic phonons remain practically not affected by small concentration of defects [40, 41]. Thus, such tiny effects due to low defect content is likely to be hidden in the INS experimental spectra of GeTe. Despite a visible change of the phonon spectral patterns below and above the structural phase transition, the local structure of GeTe seems to be retained across and far above the $R3m \leftrightharpoons Fm\bar{3}m$ phase transformation. Likewise in the recent EXAFS or high-energy total X-ray scattering studies, only a gradual increase of short and reduction of long Ge-Te bonds could be observed. The main reasons of the essentially different pictures for the local structure of GeTe above the phase transition, given by the standard diffraction and local probe methods, have been already widely discussed [6, 7, 10, 11]. Here we only remind that the conventional neutron or X-ray diffraction methods, which are based on Rietveld refinement involving only Bragg intensities, lack information contained in the background diffuse scattering and hence yield results related to the average rather than to a local structure. Despite the present experimental and theoretical investigations comply with those reported by local probe methods in predicting the presence of structural lattice distortions above T_c, the character of phase transition (displacive or order-disorder) in GeTe has not been quantified and still remains an open issue.

Acknowledgements D. Legut, VSB-Technical University of Ostrava, Czech Republic is acknowledged for technical assistance. This work was supported by the IT4Innovations national supercomputing center VSB-Technical University of Ostrava, Czech Republic - *Path to Exascale* project No. CZ.02.1.01/0.0/0.0/16_013/0001791 and IT4Innovations Excellence in Science LQ1602 project. The Interdisciplinary Center for Mathematical and Computational Modeling (ICM), Warsaw University, Poland is acknowledged for providing computer facilities under Grants No. G28-12 and No. GB70-12.

References

1. M. Wuttig and N. Yamada, Phase-change materials for rewriteable data storage, *Nat. Mater.* 6(11), 824 (2007)
2. S. Raoux, F. Xiong, M. Wuttig, and E. Pop, Phase change materials and phase change memory, *MRS Bull.* 39(08), 703 (2014)
3. L. Wang, L. Tu, and J. Wen, Application of phase-change materials in memory taxonomy, *Sci. Technol. Adv. Mater.* 18(1), 406 (2017)
4. E. F. Steigmeier and G. Harbeke, Soft phonon mode and ferroelectricity in GeTe, *Solid State Commun.* 8(16), 1275 (1970)
5. T. Chattopadhyay, J.X. Boucherele, and H. von Schnering, Neutron diffraction study on the structural phase transition in GeTe, *J. Phys. C* 20(10), 1431 (1987)
6. P. Fons, A. V. Kolobov, M. Krbal, J. Tominaga, K. S. Andrikopoulos, S. N. Yannopoulos, G. A. Voyiatzis, and T. Uruga, Phase transition in crystalline GeTe: Pitfalls of averaging effects, *Phys. Rev. B* 82(15), 155209 (2010)
7. T. Matsunaga, P. Fons, V. Kolobov, J. Tominaga, and N. Yamada, The order-disorder transition in GeTe: Views from different length-scales, *Appl. Phys. Lett.* 99(23), 231907 (2011)
8. F. Kadlec, C. Kadlec, P. Kužel, and J. Petzelt, Study of the ferroelectric phase transition in germanium telluride using time-domain terahertz spectroscopy, *Phys. Rev. B* 84(20), 205209 (2011)
9. M. J. Polking, J. J. Urban, D. J. Milliron, H. Zheng, E. Chan, M. A. Caldwell, S. Raoux, C. F. Kisielowski, J. W. III Ager, R. Ramesh, and A. P. Alivisatos, Size-dependent polar ordering in colloidal GeTe nanocrystals, *Nano Lett.* 11(3), 1147 (2011)
10. J. Hudspeth, T. Chatterji, S. Billinge, and S. Kimber, Unifying local and average structure in the phase change material GeTe, arXiv: 1506.08944 (2015)
11. T. Chatterji, C. Kumar, and U. D. Wdowik, Anomalous temperature-induced volume contraction in GeTe, *Phys. Rev. B* 91(5), 054110 (2015)
12. G. Kalra and S. Murugavel, The role of atomic vacancies on phonon confinement in a-GeTe, *AIP Adv.* 5(4), 047127 (2015)
13. D. Yang, T. Chatterji, J. A. Schiemer, and M. A. Carpenter, Strain coupling, microstructure dynamics, and acoustic mode softening in germanium telluride, *Phys. Rev. B* 93(14), 144109 (2016)
14. M. Sist, H. Kasai, E. M. J. Hedegaard, and B. B. Iversen, Role of vacancies in the high-temperature pseudodisplacive phase transition in GeTe, *Phys. Rev. B* 97(9), 094116 (2018)
15. S. D. Gupta, G. V. Varada, and G. S. Agarwal, Surface plasmons in two-sided corrugated thin films, *Phys. Rev. B* 36(12), 6331 (1987)
16. J. Raty, V. Godlevsky, P. Ghosez, C. Bichara, J. Gaspard, and J. Chelikowsky, Evidence of a reentrant Peierls distortion in liquid GeTe, *Phys. Rev. Lett.* 85(9), 1950 (2000)
17. R. Shaltaf, X. Gonze, M. Cardona, R. K. Kremer, and G. Siegle, Lattice dynamics and specific heat of a-GeTe: Theoretical and experimental study, *Phys. Rev. B* 79(7), 075204 (2009)
18. A. J. Bevolo, H. R. Shanks, and D. E. Eckels, Molar heat capacity of GeTe, SnTe, and PbTe from 0.9 to 60 K, *Phys. Rev. B* 13(8), 3523 (1976)
19. J. Raty, P. Noé, G. Ghezzi, S. Maitrejean, C. Bichara, and F. Hippert, Vibrational properties and stabilization mechanism of the amorphous phase of doped GeTe, *Phys. Rev. B* 88(1), 014203 (2013)
20. U. D. Wdowik, K. Parlinski, S. Rols, and T. Chatterji, Soft-phonon mediated structural phase transition in GeTe, *Phys. Rev. B* 89(22), 224306 (2014)

21. K. Jeong, S. Park, D. Park, M. Ahn, J. Han, W. Yang, H. S. Jeong, and M. H. Cho, Evolution of crystal structures in GeTe during phase transition, *Sci. Rep.* 7(1), 955 (2017)
22. Đ. Dangić, A. R. Murphy, É. D. Murray, S. Fahy, and I. Savić, Coupling between acoustic and soft transverse optical phonons leads to negative thermal expansion of GeTe near the ferroelectric phase transition, *Phys. Rev. B* 97(22), 224106 (2018)
23. R. Mittal, M. K. Gupta, S. L. Chaplot, M. Zbiri, S. Rols, H. Schober, Y. Su, T. Brueckel, and T. Wolf, Spin-phonon coupling in $K_{0.8}Fe_{1.6}Se_2$ and KFe_2Se_2: Inelastic neutron scattering and *ab initio* phonon calculations, *Phys. Rev. B* 87(18), 184502 (2013)
24. H. Schober, A. Tölle, B. Renker, R. Heid, and F. Gompf, Microscopic dynamics of A ^{60}C compounds in the plastic, polymer, and dimer phases investigated by inelastic neutron scattering, *Phys. Rev. B* 56(10), 5937 (1997)
25. S. W. Lovesey, Theory of Neutron Scattering from Condensed Matter, Clarendon Press, 1986
26. G. L. Squires, Introduction to the Theory of Thermal Neutron Scattering, Dover Publications, 1997
27. V. F. Sears, Neutron scattering lengths and cross sections, *Neutron News* 3(3), 26 (1992)
28. U. D. Wdowik, K. Parlinski, T. Chatterji, S. Rols, and H. Schober, Lattice dynamics of rhenium trioxide from the quasiharmonic approximation, *Phys. Rev. B* 82(10), 104301 (2010)
29. G. Kresse and J. Furthmüller, Efficient iterative schemes for *ab initio* total-energy calculations using a plane-wave basis set, *Phys. Rev. B* 54(16), 11169 (1996)
30. G. Kresse and J. Furthmüller, Efficiency of *ab-initio* total energy calculations for metals and semiconductors using a plane-wave basis set, *Comput. Mater. Sci.* 6(1), 15 (1996)
31. G. Kresse and J. Hafner, *Ab initio* molecular dynamics for liquid metals, *Phys. Rev. B* 47(1), 558 (1993)
32. J. P. Perdew, K. Burke, and M. Ernzerhof, Generalized gradient approximation made simple, *Phys. Rev. Lett.* 77(18), 3865 (1996)
33. J. P. Perdew, K. Burke, and M. Ernzerhof, Generalized gradient approximation made simple [*Phys. Rev. Lett.* 77, 3865 (1996)], *Phys. Rev. Lett.* 78(7), 1396 (1997)
34. P. E. Blöchl, Projector augmented-wave method, *Phys. Rev. B* 50(24), 17953 (1994)
35. G. Kresse and D. Joubert, From ultrasoft pseudopotentials to the projector augmented-wave method, *Phys. Rev. B* 59, 1758 (1998)
36. S. H. Garofalini, Molecular dynamics simulation of the frequency spectrum of amorphous silica, *J. Chem. Phys.* 76(6), 3189 (1982)
37. T. Róg, K. Murzyn, K. Hinsen, and G. R. Kneller, *n* Moldyn: A program package for a neutron scattering oriented analysis of molecular dynamics simulations, *J. Comput. Chem.* 24(5), 657 (2003)
38. D. B. Zhang, T. Sun, and R. M. Wentzcovitch, Phonon quasiparticles and anharmonic free energy in complex systems, *Phys. Rev. Lett.* 112(5), 058501 (2014)
39. T. Sun, D. B. Zhang, and R. M. Wentzcovitch, Dynamic stabilization of cubic $CaSiO_3$ perovskite at high temperatures and pressures from *ab initio* molecular dynamics, *Phys. Rev. B* 89(9), 094109 (2014)
40. U. D. Wdowik and K. Parlinski, Lattice dynamics of cobalt-deficient CoO from first principles, *Phys. Rev. B* 78(22), 224114 (2008)
41. U. D. Wdowik and K. Parlinski, Lattice dynamics of Fe-doped CoO from first principles, *J. Phys.: Condens. Matter* 21(12), 125601 (2009)